PHYSICAL REVIEW B **76**, 180405(R) (2007)

Fast magnetic resonance force microscopy with Hadamard encoding

Kai W. Eberhardt, Christian L. Degen,* and Beat H. Meier†
Physical Chemistry, ETH Zurich, CH-8093 Zurich, Switzerland

(Received 6 August 2007; revised manuscript received 22 October 2007; published 26 November 2007)

We present a spatial encoding technique for magnetic resonance force microscopy that allows for a much enhanced image acquisition rate. The technique uses multiplexing, based on spatial Hadamard encoding, to acquire several slices of the image simultaneously and at an undiminished signal-to-noise ratio. We demonstrate an improvement in imaging time by a factor of 7.6, and further advances can be expected.

DOI: 10.1103/PhysRevB.76.180405 PACS number(s): 76.60.Lz, 68.37.Rt, 76.60.Pc

Magnetic resonance force microscopy (MRFM)[1,2] is a new and promising method for nanoscale, noninvasive imaging. For samples in the micrometer and nanometer range the inductive detection technique of conventional magnetic resonance imaging (MRI) becomes insensitive and mechanical detection using cantilevers becomes the method of choice. Nevertheless sensitivity remains an issue[1,3] which we address here with a scheme that simultaneously samples data from many slices of the object. The scheme does not only improve the signal-to-noise ratio of the images considerably but can record ultrafast images, ultimately a complete one-dimensional or even three-dimensional image in a single scan.[4–6]

Fast acquisition methods were introduced for modern nuclear magnetic resonance (NMR) and MRI early in their development[7,8] and have indeed been crucial for their success. They take advantage of the multiplex advantage of Fourier transform spectroscopy and echo planar imaging, respectively. Ultrafast acquisition schemes in multidimensional NMR simultaneously acquire an entire time dimension by coding it into a spatial dimension.[9] In the following, we show that a Hadamard encoding technique, related to schemes previously used in MRI and NMR applications,[10–13] can be adapted for similar gains in MRFM.

The scheme—demonstrated here in one dimension (1D)—uses simultaneous encoding of several slices which would conventionally be sampled one by one. In our example, we used eight slices and observed an imaging-speed improvement of almost 8 over conventional methods with only a minor loss in signal-to-noise ratio (SNR) due to imperfections and relaxation. Significantly larger improvements of the imaging speed are undoubtedly possible.

In conventional MRFM, the image is read out by selectively detecting spins within a predefined range of resonance frequencies. Frequency and spatial position are directly related by the spatial gradient of the applied magnetic field. By shifting the frequency band in subsequent steps a 1D image of the spin density is obtained directly.

In Hadamard imaging, the signal from N slices is recorded simultaneously. The position of the spins is encoded by frequency-selective inversion pulses applied at regular intervals during signal acquisition [Fig. 1(a)], where N denotes the multiplex factor of the encoding scheme. The frequency-selective pulses for the encoding are chosen to manipulate the corresponding slices of the image according to the rows of the Hadamard matrix H_N [Fig. 1(c)]: a "+" in the matrix indicates that the magnetization of the Nth slice is in the direction of the main field, and for a "–" the slice is inverted. After N experiments, each of them providing the full signal (either positive or negative) from each slice, the intensity of the N individual slices is reconstructed using the Hadamard matrix transpose, H_N^T with $H_N^T H_N = N I_N$, where I_N is the N-by-N identity matrix.[14] After Hadamard reconstruction the signal is N times larger than from an individual experiment while the noise is $\sqrt{N}$ times larger. Therefore the SNR enhancement over the slice-by-slice method is $\sqrt{N}$, provided all measurements begin with the same initial polarization and the interruption of the detection during the Hadamard encoding pulses and the receiver deadtime is small compared to the entire detection time which, in turn, is limited by the decay time of the polarization during detection, $T_{1\rho}$. We use the higher sensitivity of the Hadamard experiment to record an image of similar quality (SNR) at a reduced imaging time.

Our experimental results image the ^{19}F spin density in a micron-sized single crystal of KPF_6 glued to a cantilever. The 1D images obtained by the conventional slice-by-slice encoding technique and by the Hadamard-8 scheme are shown in Fig. 2 as a shaded area and black curve, respectively. For the conventional curve, the image consists of 80 data points, each representing the spin density in a slice of approximately 1 μm thickness. The Hadamard-8 image acquired in only 13% of the experimental time leads to a comparable image. As seen in the two insets in Fig. 2 the noise level of the two experiments (determined predominantly by thermal noise) is roughly equivalent. A quantitative evaluation of the relative SNR of the Hadamard to the slice-by-slice measurements leads to $93 \pm 10\%$.[15] To cover the entire size of our object, ten Hadamard images were performed sequentially, from the regions indicated by the dashed vertical lines in Fig. 2. Finally, the entire image obtained with ten Hadamard-8 experiments also consists of 80 data points. Further details are discussed below.

To characterize the spatial resolution of our scheme we invert, before the imaging experiment, the magnetization in the slices 1,2, and 5,6 of the eight slices detected in the Hadamard encoded experiment. This leads to a modulation of the magnetization in the form of a square wave. Subsequently, this modulated intensity is imaged with the Hadamard-8 scheme. The image generated is shown in Fig. 3 and clearly displays the pattern previously modulated onto the magnetization, namely always two image points with positive intensity, followed by two image points with

 ©2007 The American Physical Society

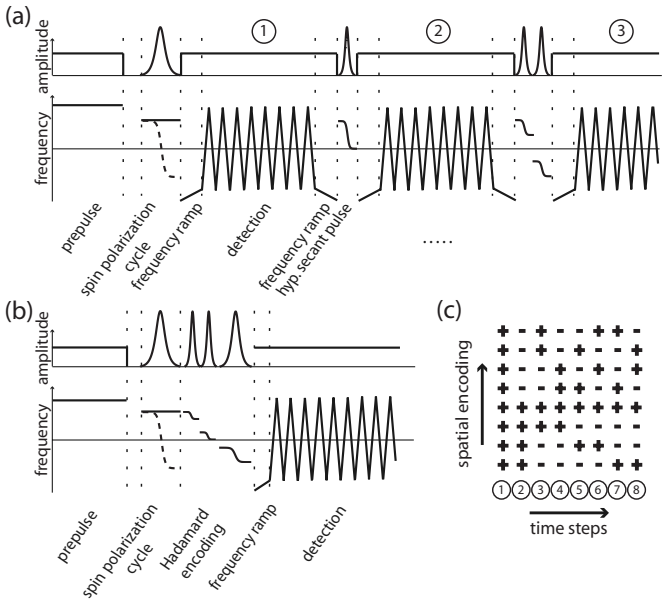

FIG. 1. (a) Pulse sequence for Hadamard-encoded imaging. The sign of the magnetization in the different slices is inverted by the frequency-selective pulses that interrupt signal detection. According to the Hadamard ($N=8$) matrix shown in (c) hyperbolic secant pulses were employed in the eight encoding steps, performed within a total time approximately equaling $T_{1\rho}$, such that sufficient signal remains for the last data point. The time periods needed for the selective pulses, where the adiabatic frequency modulation is off, were always chosen as full multiples of the cantilever period to allow the phase-sensitive reconstruction of the signal. (b) Pulse sequence for sequential Hadamard encoding. The magnetization is now encoded prior to the readout according to a column of the matrix (c), which is varied in sequential acquisitions until the magnetization of each region is acquired with all N columns. The selective pulses are applied according to a column of (c), shown here for the last time step. Sequential encoding offers the same sensitivity advantage as fast Hadamard encoding, but cannot speed up the minimum acquisition time. For both sequences a prepulse is applied to minimize the response of the cantilever to the rf for the remainder of the pulse sequence. It heats the cantilever to the temperature that it will remain at during the application of the other pulses in the sequence. Each scan is performed twice, once with the polarization inversion pulse present (dashed line) and once without it (solid line). The polarization cycle scheme is sculpted such that only the central region of the detected subslices is inverted and distinguished from the remaining signal by subtracting the two measurements in the reconstruction. This is used to differentiate between spin-signal and direct cantilever excitation by the rf and to remove the signal of the less sensitive wings of the sensitivity function (SF, see Fig. 5).

negative intensity. This experiment demonstrates that μm resolution is obtained with our Hadamard detection.

The envelope to the modulated pattern (dashed line in Fig. 3) was acquired slice-by-slice. A comparison shows that the overall crystal shape is reproduced by the modulated magnetization. We attribute the imperfections of the square wave pattern to incomplete inversion by the selective hyperbolic secant pulses, rotating-frame relaxation and to the vibration of the cantilever during the encoding. As the inversion areas are spatially fixed in the gradient field, motion of the cantilever will lead to a blurring of the inversion areas. This effect is also seen in Fig. 2, where the Hadamard image appears rougher than the slice-by-slice measurement, despite that the SNR is very similar, as seen from the noise in the areas to the sides of the crystal signal.

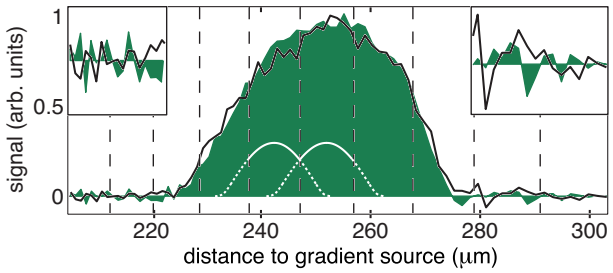

FIG. 2. (Color online) Fast acquisition 1D image (Ref. 27) (black curve). The conventional image, measured slice-by-slice (each point corresponding to a slice through the three-dimensional object) is given by the shaded area. The vertical dashed lines indicate the boundaries of the regions from which the signal was recorded simultaneously using the Hadamard scheme, termed block in the following. The sensitivity function is shown in white at the bottom of the shaded area, where contributions in the wings, ultimately removed by the polarization cycle, are indicated by dashed lines (see Fig. 5). The insets at the top magnify the sections from the noise, directly below them, vertically by 400%. A microscopic photograph of the sample is shown in Fig. 4. Hadamard encoding reduces the measurement time, at constant SNR, by a factor of 7.6.

The MRFM probe follows a sample-on-cantilever design with the oscillation of the cantilever in the direction of the gradient. The probe has already been described[16–19] and a review of the detection scheme is given by Nestle *et al.*[20] We use an iron cylinder as the gradient source (0.5 mm diameter, 10 mm length, $B_{sat}=1.75$ T). A single crystal KPF_6 sample was glued to the tip of a commercially available silicon nitride cantilever (Veeco Instruments, $k=0.01$ N/m, $f_c=832$ Hz, and $Q=12\,000$). The crystal dimensions are $\sim 40\times 40\times 80$ μm^3 (see Fig. 4).

The pulse sequence of Fig. 1 was initiated by a 0.5 s pulse 550 kHz off-resonance from the detection center to preequilibrate the temperature of the cantilever and reduce the

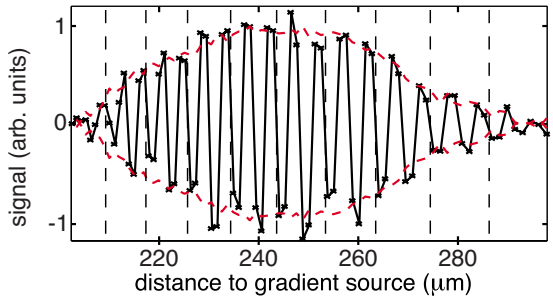

FIG. 3. (Color online) Demonstration of the spatial resolution of Hadamard encoding. Prior to the fast acquisition as shown in Fig. 1(a) the slices 1, 2, 5, and 6 of each acquisition block were inverted by selective pulses. A slice-by-slice measurement is shown as a reference as a red (gray) dashed line to both sides of the plot. The patterning of the magnetization demonstrates that the Hadamard measurement has the expected resolution (see text).

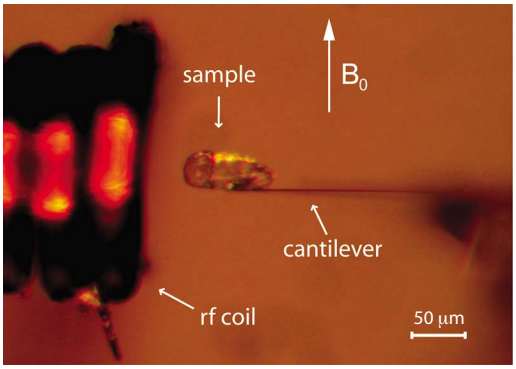

FIG. 4. (Color online) Image of the KPF_6 sample mounted on the cantilever. The direction indicating the main field is also the direction of the field gradient from the iron cylinder positioned above the sample (outside of the image). The coil was pulled back to the left from over the sample for the photograph. During an experiment the coil encloses approximately half of the sample, leaving enough room for the laser beam deflected off the bottom of the cantilever.

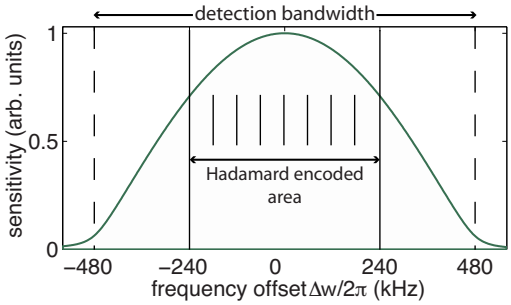

FIG. 5. (Color online) Sensitivity function of our triangular rf modulation detection scheme. The sensitivity of amplitude detection to spin packages depends on their frequency relative to the modulation center. This does not imply the physical resolution limit, ultimately given by the nuclear spin dipole-dipole interaction. By Hadamard encoding we can resolve slices much smaller than the width of the SF. The Hadamard 8 scheme does not encode the wings with low spin sensitivity and their signal was eliminated by the polarization cycle. The lines within the Hadamard-encoded area indicate the position of the slices.

rf-cantilever interactions. The rf-field amplitude corresponded to a nutation frequency of 42±5 kHz for prepulse and detection. Each detection period was 200 cantilever oscillations, corresponding to 240 ms length. The selective pulses for encoding and the polarization cycle were hyperbolic secant pulses[21] of 1 and 5 ms length, respectively, 42±5 kHz average nutation frequency, and a truncation parameter of 12. The modulation bandwidth for detection was 960 kHz. The delay between two readouts was three cantilever cycles if two encoding pulses were needed [for steps 3, 5, and 7 of Fig. 3(a)] and two cycles if only one pulse was required for encoding.

For image reconstruction the measured cantilever oscillation was first multiplied by an exponentially rising function with a time constant matched to the $T_{1\rho}$-decay of 2.3±0.5 s. Next the signal was integrated over the time between the encoding rf pulses. To avoid artifacts from the finite rise time of the cantilever ($\tau_c \approx 10$ ms using feedback damping[18,22,23]), 10 ms of the data from each detection period of 240 ms length was discarded. Next, the vector of data points was multiplied by the inverse Hadamard matrix, reconstructing the spatial information. As our detection scheme is less sensitive to spins further from the slice center,[24] the noise at the outer Hadamard slices is increased. To mitigate this effect we employed an acquisition bandwidth twice as large as the encoded area and the less-sensitive wings were removed by the polarization cycle (see Fig. 5). To compensate for the remaining effects of the sensitivity function (SF), the signal of the individual slices was divided by the SF integrated over the bandwidth of the corresponding slice.

The total acquisition time of the Hadamard measurement was 1.6 min compared to 12.1 min for the slice-by-slice measurement. Each pulse sequence was 2.5 s and between two scans there was a 2 s delay. Once per acquisition of the whole image the pulse sequence needed to be reloaded onto the wave-form generator as different pulses were required for the second part of the polarization cycle. This caused a longer delay of 10 s once per experiment. Comparing the two techniques we increased the acquisition rate by a factor of 7.6 using Hadamard matrices with $N=8$.

For the SNR considerations, we have not taken the T_1 relaxation time into account. The magnetization of an individual region has to recover between two scans that address the spins in this region. In cases where T_1 is long compared to the scan repetition time (4.5 s) multiplied by the number of Hadamard blocks (ten in our experiments), the Hadamard enhancement will be reduced. We reach the near-optimal result as T_1 of our sample is 6.2±0.3 s.

Hadamard encoding can also be performed in sequential measurements. In this case the pattern corresponding to one row of the Hadamard matrix would be encoded in subsequent scans [Fig. 1(b)]. The signal containing the encoded signal from N slices would be read out during detection for a time of several $T_{1\rho}$ without applying encoding pulses during readout. The Hadamard row for encoding will then be varied in subsequent scans until all the lines are used. In the reconstruction, the data are recombined as above, but the $T_{1\rho}$ correction is unnecessary. Hadamard encoding, in this sequential version, enhances the SNR theoretically by the same factor of $\sqrt{N}$ as the "fast" version shown in Fig. 1(a). However, it is impossible to record the image of all N slices in a single scan; N scans are needed. For SNR-limited experiments, where several scans are needed for signal averaging, sequential encoding is advantageous because it is simpler and less sensitive to artifacts.

All experiments and considerations hold for an initial equilibrium magnetization given by the Curie law (thermal ensemble). For small numbers of spins per voxel (e.g., 10^8 spins), signal detection schemes making use of the statistical fluctuations of the spin polarization have been introduced.[25] The fast acquisition scheme of Fig. 1(a) is also expected to work for these experiments.

The order N of Hadamard encoding is limited by $T_{1\rho}$ relaxation and the cantilever ring-down time $\tau_c = \frac{2Q}{\omega_c}$. In a

simple approximation $N\tau_c < T_{1\rho}$ is the limit in amplitude-modulated (AM) detection. The sequential version of Hadamard encoding is not limited by $T_{1\rho}$ and there is no apparent limit to the encoding order N. Detection methods that depend on T_1 (Ref. 26) will ease these limitations, especially as the detection time, required for each encoding step, is not limited by τ_c. Hadamard encoding can also be implemented to resolve spatial images in 3D, if suitable gradients are added to the setup.

We thank the Schweizerischer Nationalfonds, the ETH Zurich, and the Kommission für Technologie und Innovation for financial support and Andreas Hunkeler, Urban Meier, and René Verel for advice.

*Present address: IBM Research Division, Almaden Research Center, 650 Harry Road, San Jose, CA 95120, USA.
†beme@ethz.ch

[1] J. A. Sidles, J. L. Garbini, K. J. Bruland, D. Rugar, O. Zuger, S. Hoen, and C. S. Yannoni, Rev. Mod. Phys. **67**, 249 (1995).
[2] D. Rugar, R. Budakian, H. J. Mamin, and B. W. Chui, Nature (London) **430**, 329 (2004).
[3] D. Rugar, C. S. Yannoni, and J. A. Sidles, Nature (London) **360**, 563 (1992).
[4] O. Zuger, S. T. Hoen, C. S. Yannoni, and D. Rugar, J. Appl. Phys. **79**, 1881 (1995).
[5] S.-h. Chao, W. M. Dougherty, J. L. Garbini, and J. A. Sidles, Rev. Sci. Instrum. **75**, 1175 (2004).
[6] S. Tsuji, T. Masumizu, and Y. Yoshinari, J. Magn. Reson. **167**, 211 (2004).
[7] R. R. Ernst, Angew. Chem., Int. Ed. Engl. **31**, 805 (1992).
[8] P. Mansfield, Angew. Chem., Int. Ed. **43**, 5456 (2004).
[9] L. Frydman, T. Scherf, and A. Lupulescu, Proc. Natl. Acad. Sci. U.S.A. **99**, 15858 (2002).
[10] L. Bolinger and J. S. Leigh, J. Magn. Reson. (1969-1992) **80**, 162 (1988).
[11] G. Goelman, V. H. Subramanian, and J. S. Leigh, J. Magn. Reson. (1969-1992) **89**, 437 (1990).
[12] G. Goelman and J. S. Leigh, J. Magn. Reson. (1969-1992) **91**, 93 (1991).
[13] E. Kupce, T. Nishida, and R. Freeman, Prog. Nucl. Magn. Reson. Spectrosc. **42**, 95 (2003).
[14] A. Hedayat and W. D. Wallis, Ann. Stat. **6**, 1184 (1978).
[15] The SNR was calculated by dividing the maximal signal value from each of the images by the standard deviation of the noise, where it was assumed that to the sides of the signal from the crystal only noise is present (see insets of Fig. 2).
[16] C. L. Degen, Q. Lin, A. Hunkeler, U. Meier, M. Tomaselli, and B. H. Meier, Phys. Rev. Lett. **94**, 207601 (2005).
[17] Q. Lin, C. L. Degen, M. Tomaselli, A. Hunkeler, U. Meier, and B. H. Meier, Phys. Rev. Lett. **96**, 137604 (2006).
[18] C. L. Degen, U. Meier, Q. Lin, A. Hunkeler, and B. H. Meier, Rev. Sci. Instrum. **77**, 043707 (2006).
[19] D. Rugar, O. Zuger, S. Hoen, C. S. Yannoni, H. M. Vieth, and R. D. Kendrick, Science **264**, 1560 (1994).
[20] N. Nestle, A. Schaff, and W. S. Veeman, Prog. Nucl. Magn. Reson. Spectrosc. **38**, 1 (2001).
[21] M. S. Silver, R. I. Joseph, C.-N. Chen, V. J. Sank, and D. I. Hoult, Nature (London) **310**, 681 (1984).
[22] J. L. Garbini, K. J. Bruland, W. M. Dougherty, and J. A. Sidles, J. Appl. Phys. **80**, 1951 (1996).
[23] K. J. Bruland, J. L. Garbini, W. M. Dougherty, and J. A. Sidles, J. Appl. Phys. **80**, 1959 (1996).
[24] O. Zuger and D. Rugar, J. Appl. Phys. **75**, 6211 (1994).
[25] H. J. Mamin, R. Budakian, B. W. Chui, and D. Rugar, Phys. Rev. B **72**, 024413 (2005).
[26] S. R. Garner, S. Kuehn, J. M. Dawlaty, N. E. Jenkins, and J. A. Marohn, Appl. Phys. Lett. **84**, 5091 (2004).
[27] The frequency scale from the measurement is converted to the distance z to the gradient source from the known field of the cylindrical gradient source: $B_z(z) \approx \frac{B_{sat}}{2}\left(1 - \frac{z}{\sqrt{z^2+R^2}}\right)$ when the length is much larger than the radius R of the cylinder. The relationship is only accurate for the signal from the cylinder axis, but is a good approximation when the sample is off-axis by less than the radius of the cylinder.